JBIC Journal of Biological Inorganic Chemistry
https://doi.org/10.1007/s00775-023-02032-y

ORIGINAL PAPER

Bioactive apatite–wollastonite glass ceramics coating on metallic titanium for biomedical applications: effect of boron

Eren Yılmaz[1,2] · Serbülent Türk[3,4] · Alican Bahadır Semerci[5] · Mine Kırkbınar[6] · Erhan İbrahimoğlu[6] · Fatih Çalışkan[6]

Received: 19 December 2022 / Accepted: 15 November 2023

Abstract

Metallic titanium (Ti) implant surfaces need improvement for bioproperties and antibacterial behavior. For this purpose, a new boron-doped bioactive apatite–wollastonite (AW) coating was successfully developed on the Ti plate surface. The effects of boron addition on the microstructure, mechanical properties, and bioproperties of the AW coating were investigated. With the addition of boron (B), the AW coating morphology became less porous and compact. In terms of bio properties, the rate of apatite formation increased with the addition of B, and the cell viability rate increased from approximately 66–81%. B addition increased the elastic modulus of the AW coating from about 24–46 GPa and increased its hardness about 2.5 times. In addition, while no antibacterial activity was observed in the AW coating, the addition of boron slightly introduced antibacterial properties. The novel AW/B composite coating obtained is promising for Ti implant surfaces.

Graphical abstract

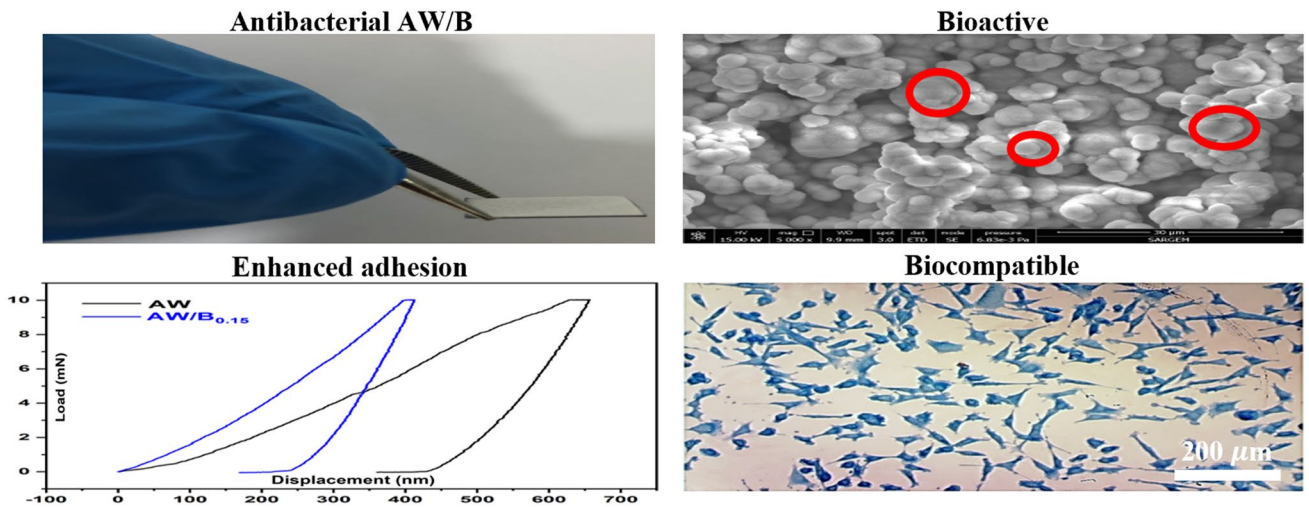

Keywords Titanium implant · Boron · Apatite–wollastonite · Coating

Introduction

Titanium (Ti) and its alloys are the most suitable candidates for bone replacement implant materials due to their load-bearing potential, non-toxicity, and biocompatibility [1–3]. However, due to their bioinert surfaces, their bonding to the surrounding living bone tissue is weak, which weakens their osseointegration feature. In addition, in terms of mechanical properties, the elastic modulus of Ti and its alloys is higher than that of bone, although low compared to other metallic materials [4]. This creates a 'stress shielding effect', leading to the problem of implant loosening [5]. In addition, Ti and its alloys do not show antibacterial properties [6].

Extended author information available on the last page of the article

Published online: 20 December 2023

These problems can be eliminated with bioactive ceramic or glass–ceramic-based coatings [7, 8]. Calcium phosphate-containing materials such as hydroxyapatite (HA) and tricalcium phosphate are the most commonly used bioactive coatings due to their high biocompatibility and ability to form apatite as a result of ion exchange reactions in body fluid [9, 10]. Previous studies have also reported that apatite–wollastonite (AW) glass ceramic induces apatite formation after implantation [11]. In these studies, wollastonite (W) was produced as a compact piece and as a coating material [12]. In the studies of Lakshmi et al. and Ming et al., respectively, W and AW were produced in bulk (in pellet form), and characterization and biocompatibility studies were carried out [13–16]. On the other hand, Bao et al. and Liu et al., in their studies, coated W on the surface of Ti and its alloys and observed the characterization and apatite formation capabilities of the coatings [17, 18]. W ($CaSiO_3$), a calcium silicate bioactive ceramic, appears to be the desired material to enhance bone tissue regeneration.

Bioactive ceramics or glass ceramics are used as fillers in many cases of significant bone loss, such as trauma, cancer, congenital abnormalities, or bone deficiency. They are also used as a coating material on metallic implant surfaces [16, 19]. However, the low fracture toughness of ceramic or glass–ceramic materials limits their use. Polymer (collagen, chitosan, etc.) or metallic ion (magnesium, silver, strontium, zinc, etc.) additives have been widely studied in recent years to improve the mechanical properties, cell behavior, and antibacterial characteristics of calcium-phosphorus-based biomaterials [20]. Boron (B), a remarkable trace element, especially in humans, is known to have numerous functions in the regulation of bone metabolism [12, 21]. In animal experiments, B supplementation has been reported to reduce the effects of vitamin D deficiency. Boron deprivation in animals leads to impaired growth and abnormal bone development. Another study showed that supplementing B as boric acid improved bone structure and strength in rats. It has also been found that daily supplementation of 1 mg/L of B in postmenopausal women significantly improves bone osteocalcin levels [22]. Therefore, researchers focused on synthesizing boron-doped HA as a candidate for biomedical applications and investigating its structural, mechanical, and biological properties. EO Tuncay et al., in their study, increased the proliferation and osteoblastic differentiation of MC3T3-E1 cells by adding B to the HA coating [23]. Aksoy et al., on the other hand, increased the adhesion strength of the coating by adding B to the HA coating and improved the corrosion resistance [24]. The number of studies in which B reinforcement was carried out on glass–ceramic-based materials is limited. Gorustovich et al. increased osseointegration and bone formation by producing 2 wt% B_2O_3 reinforced bioactive glass [25]. In the study of Deilmann et al., they increased the elastic modulus by adding B to the porous bioactive glass [26]. The antibacterial effect of B has also been proven in some studies.

In this study, B-reinforced AW coating for implant applications that can be used instead of bone to improve the bioproperties of the Ti surface was investigated. Although bioglass studies containing B in bulk form are rare in the literature, no AW coating with B content has been found. In addition, in this study, there are comprehensive studies on microstructure, phase studies, mechanical properties, and cellular and antibacterial studies, unlike previous B-reinforced bioglass studies.

Materials and method

Ti foil (Alfa Aesar) of 0.25-mm thickness was cut in dimensions of 10 mm × 10 mm as the substrate material. Before coating, Ti foils were cleaned in acetone and kept in HF acid solution of 10% by volume for 5 min to ensure the adhesion of the coating to the substrate. It was then rinsed and dried in an oven. AW powders, the primary material of each coating, were produced following the path in our previous study [27]. In summary, the raw materials of CaO, SiO_2, P_2O_5, MgO, Al_2O_3, and CaF_2 were weighed in appropriate proportions and mixed in an alumina crucible. After waiting 1 h at 1400 °C, the molten mixture was poured into the water and frit. After drying, AW powders were produced by grinding in the mill. The ethanol solution containing a certain amount of AW powder was sonicated until its viscosity increased and it became sludgy. To prevent cracking in the subsequent heat treatment and to increase the adhesion of the coating, 2% (wt) ethyl cellulose was added to the solution medium. Then the sludge was poured on the pre-treated Ti substrate, and the samples were dried in the oven at room temperature. As a final treatment, heat treatment was carried out at 800 °C (AW) to increase the adhesion strength of the coating. Three different B-added coatings were obtained by adding 5% (AW/$B_{0.05}$), 10% (AW/$B_{0.1}$), and 15% (AW/$B_{0.15}$) B_2O_3 powder to the ethanol solution containing AW powder. For B-containing coatings, the production route in the AW coating described above was followed, as shown in the flowchart in Fig. 1.

The phase contents and characterization studies of each produced coating were examined by XRD analysis (RIGAKU D/MAX 2200), FTIR analysis (Perkin Elmer), and Raman spectra (Kaiser Raman RXN1). Microstructure examinations of the coatings before and after soaking in simulated body fluid (SBF) were performed with FESEM (Quanta 450 FEG). SBF was prepared according to Kokuba's recipe, samples were incubated at 37 °C at 7.4 pH for 7 days, and the SBF was renewed daily. The chemical content, especially the change in the Ca/P ratio, after holding in SBF was interpreted by EDS analysis.

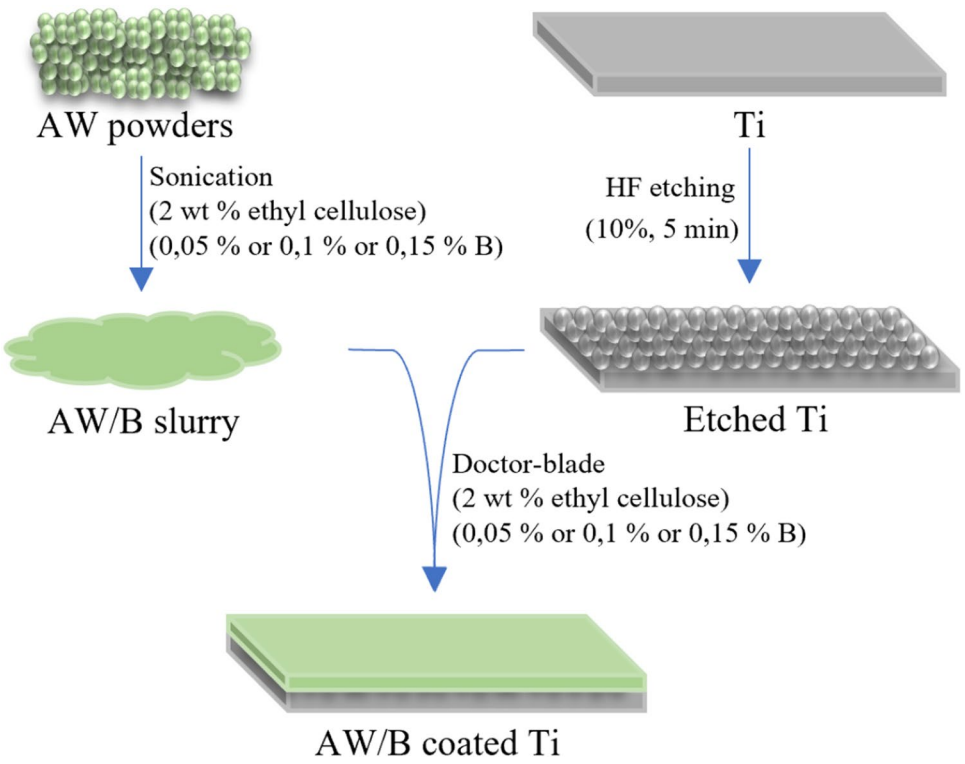

Fig. 1 Flowchart of the preparation of AW/B-coated Ti substrate

In addition, the behavior of each coating sample against NIH-3T3 mouse embryonic fibroblast cells was examined. Before cell tests, each sample was UV sterilized for 15 min. The sterilized samples were first washed with sterile phosphate buffered saline (PBS). Then two separate 24-well sterile plates were placed in the wells for cytotoxicity and cell adhesion experiments. Three of each coating sample were used for cytotoxicity and cell adhesion assay. 30,000 cells per well (in 300 µL DMEM) were seeded on the samples placed in the wells. The volume was completed to 600 µL by adding 300 µL of Dulbecco's modified Eagle medium (DMEM). Then the cultures were incubated at 37 °C in a humidified atmosphere of 5% CO2 in air for 48 h. For the adhesion test, cells were fixed with 4% paraformaldehyde and washed three times for 5 min with PBS. The samples were stained with 0.1% Giemsa, kept in the dark for 15 min, washed with PBS and viewed under a light microscope. For the cytotoxicity, at the end of the incubation period, the DMEM medium in the wells was pipetted, and 300 µL of fresh DMEM was added. 30 µL of MTT (4,5-dimethylthiazol-2-yl-2,5 diphenyltetrazolium bromide; thiazolyl blue) dye was added on it and incubated for 4 h. After 4 h of incubation, sodium dodecyl sulfate (SDS) solution was added to the wells to dissolve the formazone crystals and incubated for 12 h in an oven. Then 200 µL of each sample was transferred to a clean 96-well plate and read in a spectrophotometer at 570 nm. As a result of the study, the absorbance values obtained from the spectrophotometric measurements of the samples were evaluated, and the results were given as % cell proliferation. The images of cell adhesion experiments carried out together with cytotoxicity experiments at the end of 48 h were evaluated with light microscopy. A decrease in the number of viable cells leads to a decrease in metabolic activity in the sample. Such a reduction is directly related to the amount of blue–violet formazan formed, as monitored by the optical density (OD) at 570 nm. The following equation is used to calculate the decrease in viability compared to the negative control:

$$\text{Viab.\%} = 100 \times \frac{\text{OD570e}}{\text{OD570nc}} \quad (1)$$

OD570e is the average value of the measured optical density of 100% extracts of the test sample and OD570nc is the average value of the measured optical density of the negative control. A lower Viab.% value means higher cytotoxicity. The rate of cytotoxicity is graded based on cell viability; non-cytotoxic > 90% cell viability, slightly cytotoxic = 60–90% cell viability, moderately cytotoxic = 30–59% cell viability, and severely cytotoxic = < 30% cell viability [28].

Antibacterial activities on *Escherichia coli* (*E.coli*, ATCC 8739) and *Staphylococcus aureus* (*S. aureus*) ATCC 29213 bacteria were performed by plate counting method for the produced AW coating and AW/$B_{0.15}$ sample (the sample with the highest cell viability). *S. aureus* has a high affinity for skin and bones, is the organism associated with postoperative

orthopedic infection that causes bone matrix resorption and stimulation of osteonecrosis [29]. *Escherichia coli* is one of the first causes of Gram-negative orthopedic implant infections. Gram-negative bacilli cause approximately 6–23% of all orthopedic implant infections, and *Escherichia coli* is the most frequently isolated microorganism in these cases [30]. Therefore, these two bacterial types were preferred in this study. The surfaces of the composite films were sterilized with UV light (Osram Puritec HNS S 9W G23) for 30 min. 100 µL of bacterial culture (1×10^6 CFU/mL) activated 24 h in advance was transferred to the films and covered with a polyethylene film. The films were then incubated at 90% relative humidity and 37.5 °C for 24 h. The films were washed with 20 mL of 1% peptone (Merck) water and inoculated by the spread coating method on nutrient agar (Merck). After 24 h of incubation at 37.5 °C, colonies in the medium were counted using the colony counter. Uncoated 0.25-mm thick Ti foil was used as negative control. Percent antibacterial activity was calculated according to Eq. 2.

$$A = [(B - S)/B] \times 100 \quad (2)$$

where A is the antibacterial effect (%), B is the average number of bacteria colonies on the control (without AW/$B_{0.15}$), and S is the average number of bacteria colonies in the test sample (AW/$B_{0.15}$).

For the AW/$B_{0.15}$ sample, which gave the best bioproperty results, the hardness and elastic modulus examinations were carried out with the nanoindentation test Berkovich recessed tip. In addition, the mechanical properties of the AW sample were also investigated for comparison.

Results and discussion

XRD patterns of AW and boron-doped AW coatings are given in Fig. 2a. For each coating, it can be said that the surface of the Ti substrate is completely covered since the peak of Ti is not visible (Figure S1). The maximum peak of AW appeared at approximately $2\theta = 30°$ for all coating samples. The existence of the AW phase has been proven, consistent with the studies in the literature [17, 31]. The XRD patterns of the boron-doped coatings were similar to those of the AW coating, no significant change was observed. A similar situation was reported in another study in which boron was added to HA [23]. In the study of Tunçay et al., there was no significant change in XRD peaks with the addition of boron to HA. The presence of boron in the coatings has been proven by FESEM, EDS, FTIR, and RAMAN analyses.

Figure 3 shows the surface morphology images of each coating before and after soaking in SBF. FESEM images were taken at the same magnification (5000×). No cracks were detected on the coated sample surfaces, and a homogeneous morphology was observed (Fig. 3a1–d1). Here, it can be thought that slow heating and slow cooling steps (10 °C/min) are effective in the heat treatment applied after coating. The coating thicknesses were measured similarly because the coatings were carried out with the same method, and therefore the cross-sectional FESEM image of the AW/B0.10 coating is presented in the supplementary (Figure S3). It has been observed that the average coating thickness of 55.58 µm is in the appropriate range for implant material coatings used in the biomaterial field [32]. The AW-coated sample surface consisted of particles in the 1–8.5 µm. With the addition of boron to AW, this particle form disappeared, and the particles were fused to give an irregular morphology. Boron supplementation to AW improved the surface morphology by providing increased adhesion between particles. ME Aksoy et al. reported that boron addition provides better interconnection between grains and pores in their study of boron-doped HA coating [24]. As boron was added to AW, the interparticle pores decreased, and a more rigid morphology was formed. A similar effect was reported in the studies of A. E. Pazarçeviren et al. examining the addition of boron to HA [33]. After the coated samples were kept in SBF for 7 days, 3–6.5-µm spherical apatite particles (indicated by red circles) were formed on their surfaces (Fig. 3a2–d2). Especially in boron-added coatings, the diameter of apatite spherical particles increased compared to AW coating, and the surface was covered entirely with spherical particles. It has also been reported in the literature that boron accelerates apatite precipitation in SBF [34]. The ability of the apatite particles to form showed that the coatings had excellent mineralization ability and good bioactivity.

The EDS results obtained from the coating surfaces before and after holding in SBF are given in Table S1. Ca, Si, P, Mg, Al, and O elements due to the presence of AW were detected in all samples. In addition to these elements, there is element B in boron-added coatings. A sharp decrease was observed in the Si concentration of wollastonite due to the formation of an apatite layer in the coatings kept in SBF. In addition, the Ca/P ratio (between 1.59–1.95) after soaking in SBF approached the stoichiometric ratio of apatite (range 1.67) compared to pre-incubation in SBF (between 5.53–5.95) [35]. In some studies in the literature, the apatite formation ability of wollastonite-based coatings has been confirmed. For the mechanism of apatite formation on the W coating, it was suggested that after immersion in SBF, the calcium ions were initially exchanged with H^+, and silanol (Si–OH) formed on the layer surface, and an increase in the pH value at the coating–SBF interface. As a result, a negatively charged surface with a functional group (Si–O) is formed on the surface. Due to the negatively charged surface, the Ca^{2+} ions in the SBF solution are attracted to the interface between the coating and the solution. Thus, the ionic activity of apatite at the interface increases as apatite

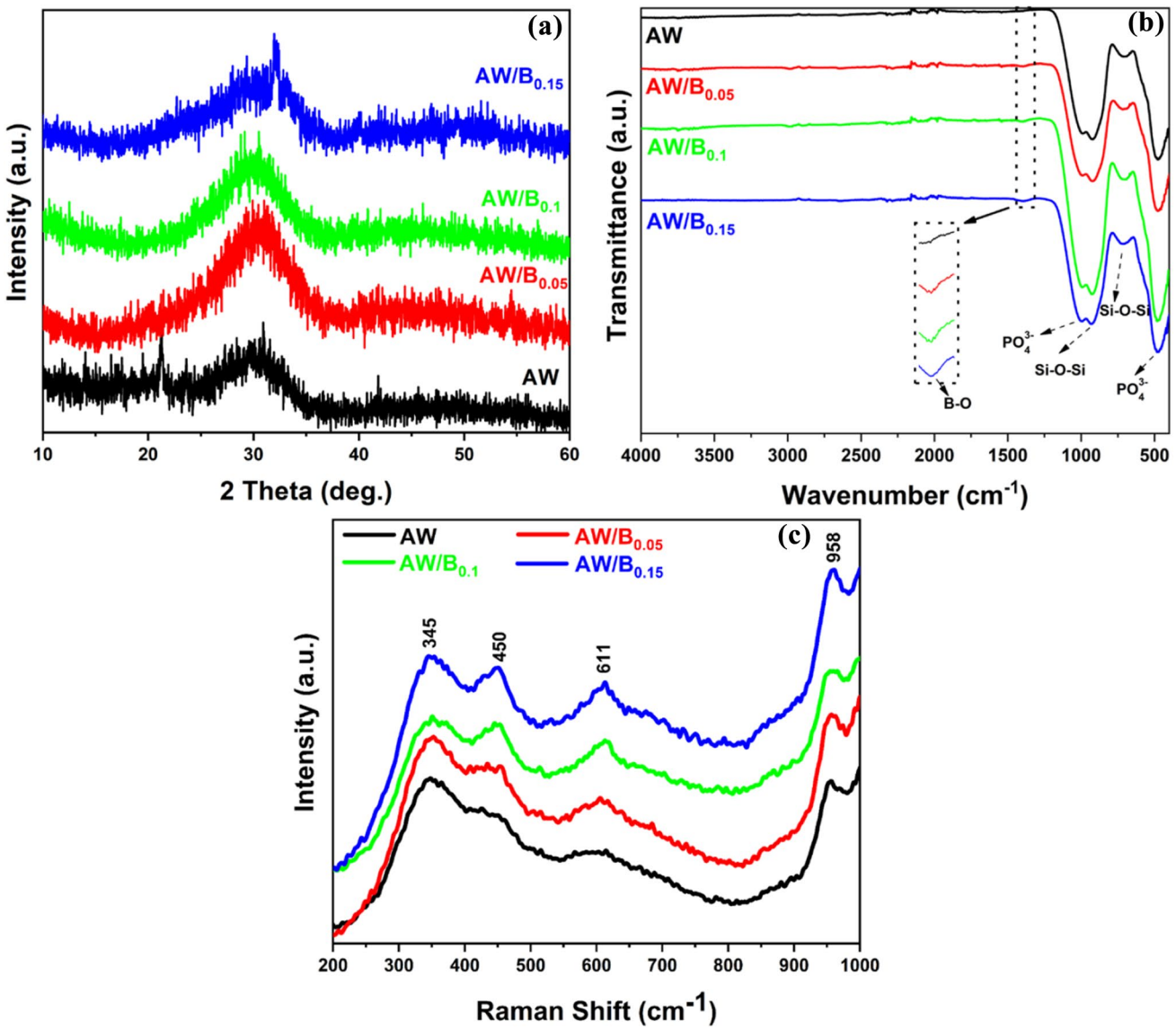

Fig. 2 **a** XRD spectra, **b** FTIR spectra, and **c** RAMAN spectra of AW, AW/$B_{0.05}$, AW/$B_{0.1,}$ and AW/$B_{0.15}$ coatings

precipitates on the coating surface [18, 31, 36–38]. The critical point here is apatite formation on the negatively charged functional group surface (Si–O). According to the literature, W partially dissolves in SBF and promotes apatite formation [39].

FTIR spectra of the coatings are shown in Fig. 2b. Characteristic absorption bands due to the presence of apatite and W were observed for each coating. Bands at about 550 cm^{-1} (ν_4; PO_4^{3-}; asymmetrical O–P–O bending) and 1030 cm^{-1} (ν_3; PO_4^{3-}) are associated with phosphate groups. Absorption bands caused by Si–O–Si asymmetric stretching vibration and Si–O–Si symmetric stretching vibration are observed in the range of 900 cm^{-1} and 750 cm^{-1}, respectively [40]. Significant peaks in the FTIR spectrum prove the presence of AW and are compatible with XRD analysis. In addition, the calcium carbonate peak reported in the FTIR analysis of W or HA-based coatings in the literature was not observed in this study. It is thought that due to the heat treatment after coating, calcium participates in forming W, and CO_2 gas is removed. In addition, around 1450 cm^{-1}, the adsorption band attributed to B–O stretching vibration for boron-doped coatings appeared [41].

A more detailed examination of the chemical characterization composition of the coatings was carried out by Raman analysis. For each coating, Raman bands at 345 cm^{-1} and 958 cm^{-1} are associated with the W phase, while 611 cm^{-1} Raman bands correspond to the phosphate group [42]. A band appeared at 450 cm^{-1} in boron-added coatings. This band is attributed to O–B–O bending (Fig. 2c) [23]. According to the results and analyses obtained, and in the light of

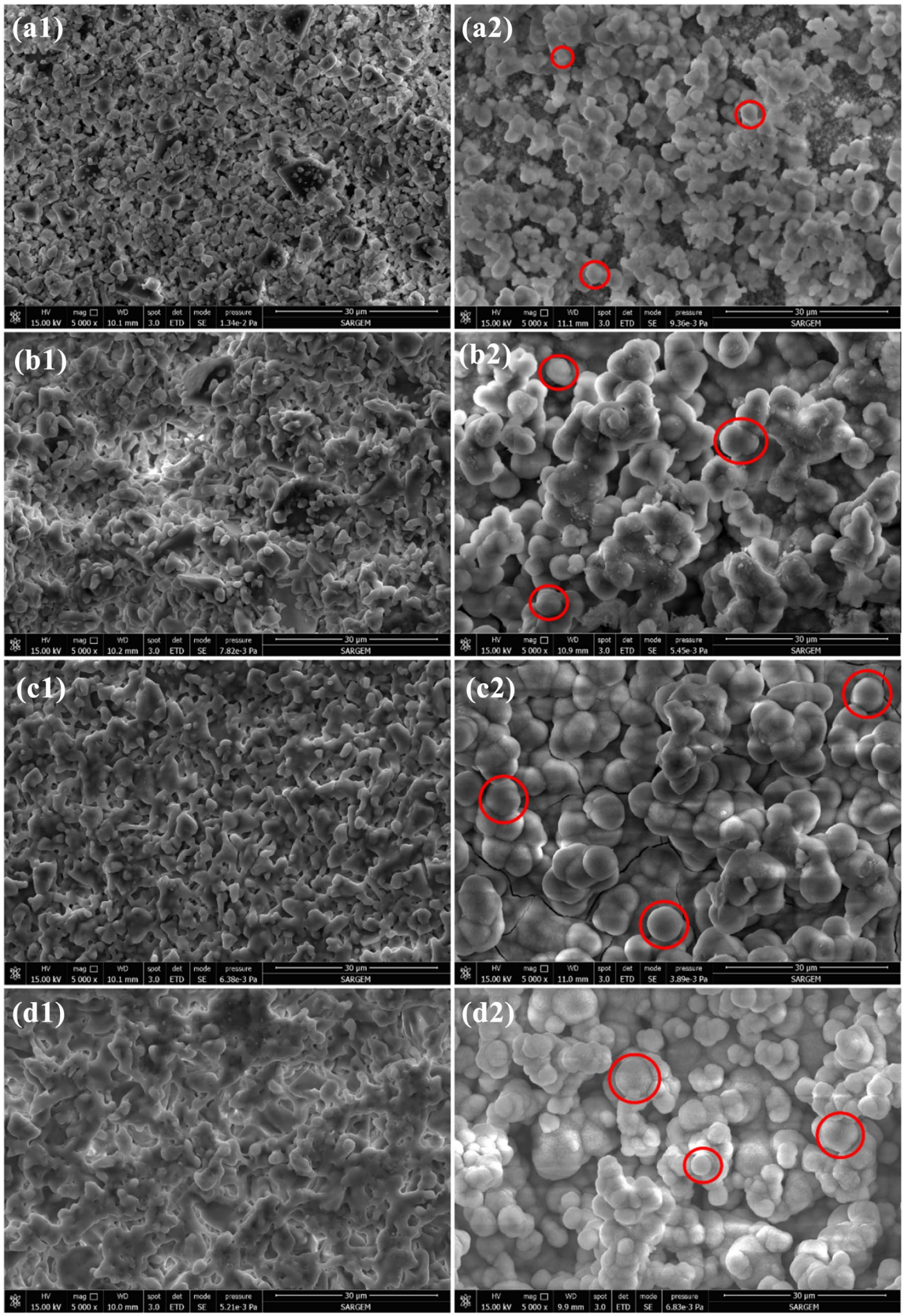

Fig. 3 FESEM images of AW (**a1**), AW/$B_{0.05}$ (**b1**), AW/$B_{0.1}$ (**c1**), AW/$B_{0.15}$ (**d1**) before soaking in SBF and FESEM images of AW (**a2**), AW/$B_{0.05}$ (**b2**), AW/$B_{0.1}$ (**c2**), AW/$B_{0.15}$ (**d2**) after soaking in SBF for 7 days

the literature, the interaction model on the AW/B surface and the Ti surface was established during the preparation of the AW/B-coated Ti substrate and shown in Scheme 1.

The most important feature expected from implants in the body is their compatibility with the surrounding cells and tissues. In cell tests, no cytotoxic effect was observed in any of the coating samples. As B was added to AW, the cell proliferation rate on the coating surface increased from approximately 64–82% (Table 1). Cell adhesion images on coated surfaces are consistent with cell viability rates (Fig. 4). The highest cell adhesion rate was observed in the $AW/B_{0.15}$ sample. In addition, branched images of cells show that they are alive. The results are also consistent with the apatite formation capabilities of the coatings (Fig. 3). New bone cell formation begins with the condensation of mesenchymal progenitor cells, followed by the differentiation of cells. The mitogen-activated protein kinase (MAPK) signaling pathway regulates many aspects of bone development and maintenance. The literature has reported that boron in the form of H_3BO_3 potently activates the MAPK signaling pathway to markedly increase cell proliferation and growth at low concentrations [25]. Many of these signaling cascades have been shown to be required for mesenchymal cell attachment, osteoblast differentiation, and proliferation. MAPKs are evolutionarily conserved enzymes that convert extracellular stimuli into a wide variety of cellular responses. MAPK has a critical role in cell proliferation and differentiation. This effect of boron was demonstrated by cell viability rates and cell adhesion images (Fig. 4, Table 1). In the literature, the positive effects of boron on bone development and preservation at the clinical level have been mentioned.

Ti implants used as bone substitutes are susceptible to bacterial contamination during and after the operation, leading to an inflammatory process in the surrounding tissues. Bacteria attached to the implant surface form a biofilm.

Table 1 Viability of 3T3 fibroblast cells cultured on AW, $AW/B_{0.05}$, $AW/B_{0.1}$, and $AW/B_{0.15}$ coatings

Cell viability of samples (%)			
AW	$AW/B_{0.05}$	$AW/B_{0.1}$	$AW/B_{0.15}$
63.62	66.76	74.54	81.99

Biofilm protects bacteria from the external environment. Biofilm inhibits the attachment and growth of eukaryotic cells, compromising soft tissue healing and bone apposition. Implant failure and removal is the only effective treatment in most cases, as bacteria in the biofilm are protected from host defense and oral antibiotic treatments [43]. A promising approach to prevent biofilm formation from a very early stage is using bactericidal surfaces. Bactericidal surfaces can prevent bacterial attachment and proliferation due to antibiotic administration or in the presence of specific bactericidal agents. The prophylactic use of the antibiotic may have some disadvantages, such as a high release rate in the first h, possible ineffective concentration, and patient exposure to the drug. Surfaces doped with bactericidal elements (such as silver, copper, and zinc) are being developed to overcome the limitations of antibiotic delivery. However, other bactericidal features need to be investigated to prevent long-term complications from the toxicity of these elements. Bactericidal agents, such as boron, that control communication between bacteria are preferred over other bactericidal agents since bacterial resistance is less likely to occur. Some opinions about the antibacterial mechanism of boron are presented in the literature. Boric acid is believed to have the ability to penetrate cell membranes and show any antimicrobial activity. It has also been mentioned that boron compounds can react with hydroxyl-rich compounds such as phospholipids, lipopolysaccharides, and glycoproteins in

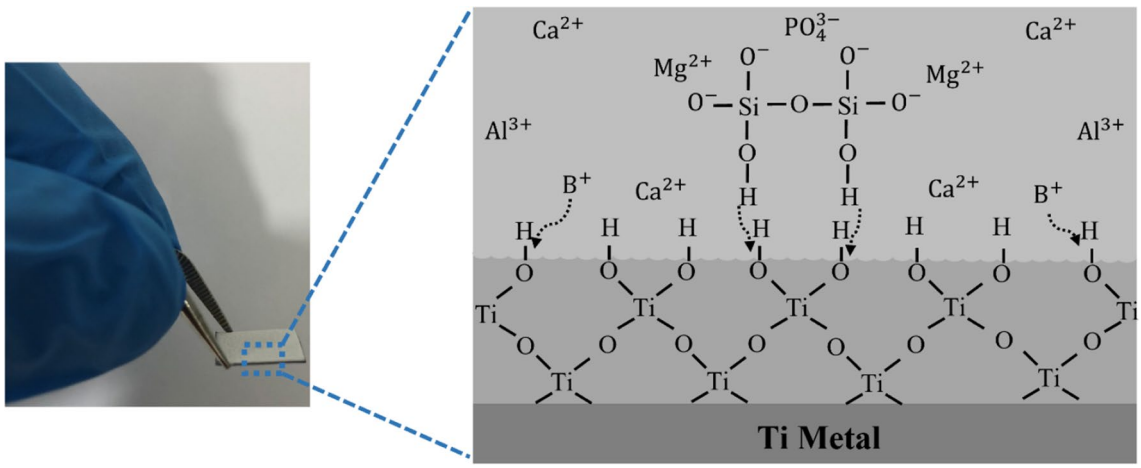

Scheme 1. AW/BA-coated sample and schematic illustration of the mechanism of AW/B coating on Ti substrate

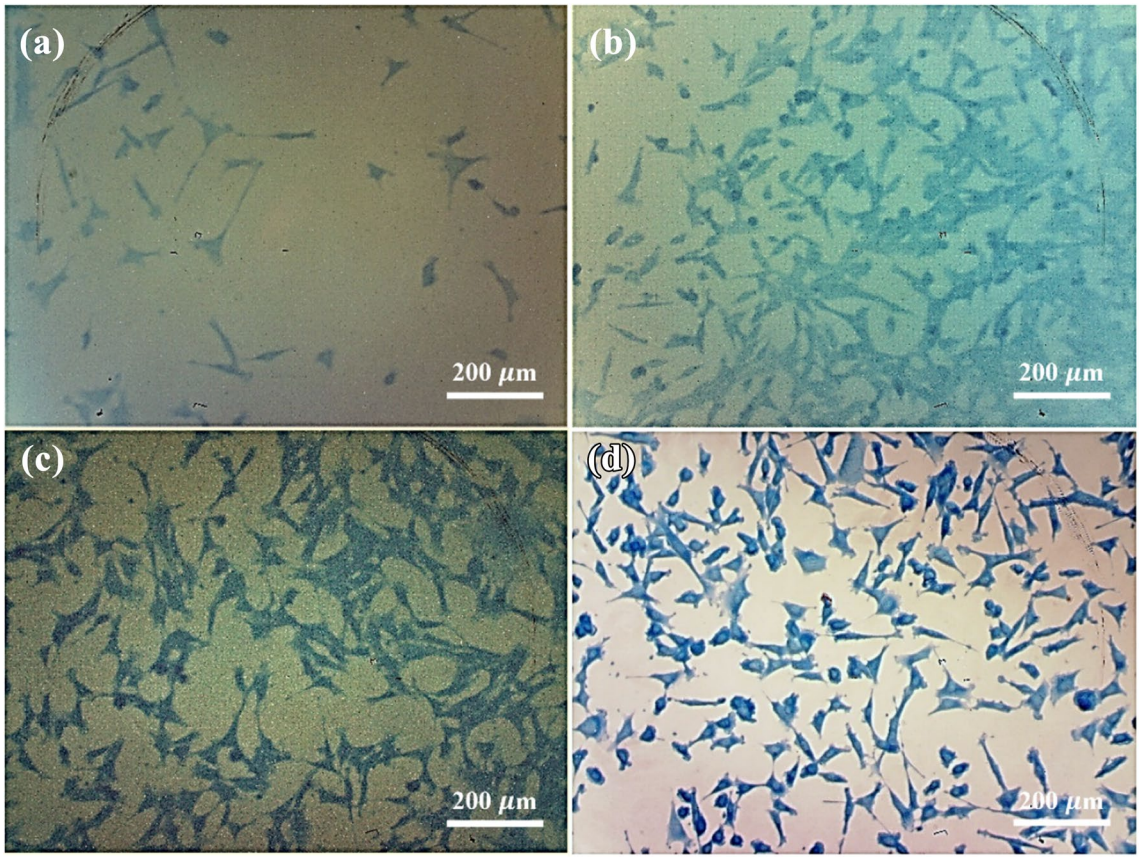

Fig. 4 Optical micrographs of the attached 3T3 fibroblast cells on the **a** AW, **b** AW/$B_{0.05}$, **c** AW/$B_{0.1}$, and **d** AW/$B_{0.15}$ coatings

Table 2 Antibacterial activity (%) of AW, AW/$B_{0.05}$, AW/$B_{0.1}$, and AW/$B_{0.15}$ coatings

Samples	Antibacterial activity (%)	
	E. coli	*S. aureus*
AW	0	0
AW/$B_{0.15}$	7.8	4.5
N. kontol	0	0

microbial membranes. Such interactions can cause membrane functional activity changes, including membrane-associated enzymes. The mode of action of boric acid has been summarized as inhibition of membrane proteins and inhibition of enzymes and coenzymes within the cell. Inhibition of membrane proteins, including enzymes responsible for active transport, and interference with membrane structures can inhibit nutrient transport and uptake and slow down the metabolic processes of microorganisms [44].

As a result of the antibacterial analysis, sample AW/$B_{0.15}$ exhibited antibacterial activity in wound healing against two possible sources of infection, such as *S. aureus* and *E. coli* (Table 2). It was revealed that AW-coated and blank films used as control did not show any activity, while AW/$B_{0.15}$-coated films showed a certain amount of bactericidal effect. The highest activity was determined in the coating containing AW/$B_{0.15,}$ with 7.8% for *E. coli* and 4.5% for *S. aureus*. This can be attributed to the thinner cell wall of *E. coli* than *S. aureus*. In Table 2, it was seen that antibacterial activity increased depending on the increase in boron concentration. In parallel with this study, Wang et al. determined that the antibacterial activity of boron-doped TiO2 nanoparticles increased depending on the boron concentration [45]. There are limited studies on the antibacterial activities of boron-added coating materials. In a study investigating the antibacterial activity of boron-doped TiO_2 coatings, it was observed that the coating produced on *S. aureus* exhibited a killing rate of about 6%, similar to our study [46]. Another study evaluating the antibacterial activity of textile materials coated with nanoboron particles reported that the produced coated surfaces limited the growth of *E. coli* and *S. aureus* bacteria [47]. The antimicrobial results in this study clarified that the AW/$B_{0.15}$ coating has some bactericidal effect against *E. coli* and *S. aureus*. These results are promising for biomaterials to be developed with boron. We continue and work to produce coatings with antimicrobial activity to

appropriately improve the boron dose and explain the tubing's interactions with different metal combinations.

One of the most critical problems of intraosseous Ti implants is that they have a high elastic modulus compared to bone. The compatibility of the elastic modulus with the bone is important to minimize the undesirable complication of stress-protective osteolysis caused by the unbalanced stress distribution between the bone and the implant. In the literature, mechanical properties compatible with bone have been achieved in HA-based coatings. Data on the mechanical properties of AW and AW/$B_{0.15}$ coatings are given in Fig. 5. The elastic modulus and hardness of the AW and AW/$B_{0.15}$ coatings were measured as 24.6 GPa, 46.3 GPa, and 1692 MPa, 4304 MPa, respectively. Considering the load–penetration depth curves of the coatings, the penetration depths of AW and AW/$B_{0.15}$ coatings under 10 mN load are approximately 6×10^2 nm and 3.5×10^2 nm, respectively (Fig. 5). As the hardness increases, the depth of penetration decreases [48]. The AW/$B_{0.15}$ coating has a higher resistance to indentation than the AW coating. Addition of B to AW increased hardness and E. The elastic modulus of both coatings is compatible with that of cortical bone (10–30 GPa). The effect of B addition on mechanical properties can be explained by microstructure images (Fig. 3). With the addition of B to AW, better bonding between the particles in the coating morphology and decreased porosity affected the improvement of mechanical properties. In addition, it can be thought that the grain size reducing the effect of B may contribute to the advancement of mechanical properties. In the literature, as a result of the addition of B to HA with similar effects, the hardness and adhesion strength of the coating increased, while the deformation and delamination of the coating decreased.

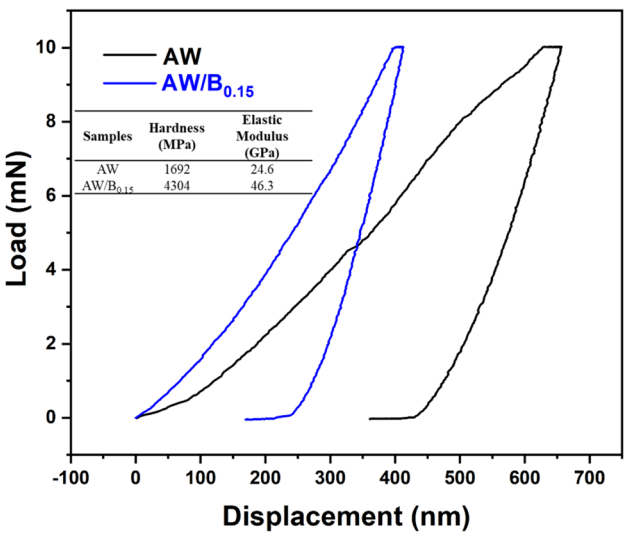

Fig. 5 Load–penetration depth curves for indents AW and AW/$B_{0.15}$ coatings

Conclusion

AW and boron-doped AW coatings were successfully applied to the Ti plate surface without deformation, delamination, or cracking. The effects of boron addition to AW on microstructure, mechanical properties, cell behavior, and antibacterial properties were investigated. The main findings can be summarized as follows:

- As boron was added to AW, the morphology of the coating changed from a particulate and porous appearance to a more compact and homogeneous structure. This change in morphology contributed to the increase in mechanical properties. The hardness and elastic modulus of the AW/$B_{0.15}$ coating were measured at 4304 MPa and 46.3 GPa, respectively, while the values of the AW coating were 1692 MPa and 24.6 GPa. Compatibility of elastic modulus values with those of cortical bone will reduce the problem of implant loosening.
- Spherical apatite particles were formed on each coated sample surface after immersion in SBF. It was observed that the addition of boron accelerated the formation of apatite. It has been proven that these produced coatings have bioactive properties.
- 3T3 fibroblast cell viability values on the surface of the coatings increased from 66.76% to 81.99% as B was added to AW. Good cell adhesion was observed in the formed biocomposite coatings.
- While no antibacterial activity was observed in the AW coating, the coating gained antibacterial properties with the addition of B.
- As a result, the B-doped AW coating is recommended for Ti implant surfaces in terms of apatite formation ability, mechanical properties, cell behavior, and antibacterial properties.

Supplementary Information The online version contains supplementary material available at https://doi.org/10.1007/s00775-023-02032-y.

Acknowledgements This work was supported by the Scientific Research Projects Commission of Sakarya Applied Sciences University (Project number: 2020-29-03-018).

Data availability Data will be made available on request.

Declarations

Conflict of interest The authors declare that they have no known competing financial interests or personal relationships that could have appeared to influence the work reported in this paper.

References

1. Aufa AN, Hassan MZ, Ismail Z (2022) Recent advances in Ti–6Al–4V additively manufactured by selective laser melting for biomedical implants: prospect development. J Alloy Compd 896:163072. https://doi.org/10.1016/j.jallcom.2021.163072
2. Yılmaz E, Çalışkan F (2022) A new functional graded dental implant design with biocompatible and antibacterial properties. Mater Chem Phys 277:1–8. https://doi.org/10.1016/j.matchemphys.2021.125481
3. Moloodi A, Toraby H, Kahrobaee S et al (2021) Evaluation of fluorohydroxyapatite/strontium coating on titanium implants fabricated by hydrothermal treatment. Prog Biomater 10:185–194. https://doi.org/10.1007/s40204-021-00162-7
4. Seesala VS, Dhara S (2022) A novel strategy for fabricating zirconia implants with a trabecular biomimetic porous surface. J Am Ceram Soc 105:5131–5139. https://doi.org/10.1111/jace.18504
5. Guo Y, Chen D, Cheng M et al (2013) The bone tissue compatibility of a new $Ti_{35}Nb_2Ta_3Zr$ alloy with a low Young's modulus. Int J Mol Med 31:689–697. https://doi.org/10.3892/ijmm.2013.1249
6. Si Y, Liu H, Yu H et al (2022) MOF-derived CuO@ZnO modified titanium implant for synergistic antibacterial ability, osteogenesis and angiogenesis. Colloids Surf B Biointerfaces 219:112840. https://doi.org/10.1016/j.colsurfb.2022.112840
7. Yılmaz E (2021) Modification of the micro arc-oxidized Ti surface for implant applications. J Bionic Eng 18:1391–1399. https://doi.org/10.1007/s42235-021-00101-z
8. Bargavi P, Chandran RR, Durgalakshmi D et al (2022) Drug infused Al_2O_3-bioactive glass coatings toward the cure of orthopedic infection. Prog Biomater 11:79–94. https://doi.org/10.1007/s40204-022-00181-y
9. Singh P, Bansal A, Verma VK (2022) Hydroxyapatite reinforced surface modification of SS-316L by microwave processing. Surf Interfaces 28:101701. https://doi.org/10.1016/j.surfin.2021.101701
10. Khvostov MV, Bulina NV, Zhukova NA et al (2022) A study on biological properties of titanium implants coated with multi-substituted hydroxyapatite. Ceram Int. https://doi.org/10.1016/j.ceramint.2022.08.067
11. Liu X, Ding C (2002) Morphology of apatite formed on surface of wollastonite coating soaked in simulate body fluid. Mater Lett 57:652–655
12. Qin W, Kolooshani A, Kolahdooz A et al (2021) Coating the magnesium implants with reinforced nanocomposite nanoparticles for use in orthopedic applications. Colloids Surf A Physicochem Eng Aspect 621:126581. https://doi.org/10.1016/j.colsurfa.2021.126581
13. Çalişkan F (2016) Apatite wollastonite-reinforced hydroxyapatite biocomposites. Acta Phys Polon A 129:665–668. https://doi.org/10.12693/APhysPolA.129.665
14. Lakshmi R, Sasikumar S (2015) Influence of needle-like morphology on the bioactivity of nanocrystalline wollastonite—an in vitro study. Int J Nanomed 10:129–136. https://doi.org/10.2147/IJN.S79986
15. Ming X, Ou J, Zhou D et al (2007) Preparation and properties of porous apatite-wollastonite bioactive glass-ceramic. Key Eng Mater 332:169–172. https://doi.org/10.4028/www.scientific.net/KEM.330-332.169
16. Tatli Z, Bretcanu O, Çalıs F, Dalgarno K (2022) Fabrication of porous apatite-wollastonite glass ceramics using a two steps sintering process. Mater Today Commun 30:1–6. https://doi.org/10.1016/j.mtcomm.2022.103216
17. Bao Q, Zhao K, Liu J (2012) Characterization of wollastonite coatings prepared by sol–gel on Ti substrate. J Coat Technol Res 9:189–193. https://doi.org/10.1007/s11998-009-9236-7
18. Liu X, Ding C, Chu PK (2004) Mechanism of apatite formation on wollastonite coatings in simulated body fluids. Biomaterials 25:1755–1761. https://doi.org/10.1016/j.biomaterials.2003.08.024
19. Yılmaz E, Gökçe A, Findik F, Ho G (2018) Metallurgical properties and biomimetic HA deposition performance of Ti–Nb PIM alloys. J Alloy Compd 746:301–313. https://doi.org/10.1016/j.jallcom.2018.02.274
20. Wei S, Ma J, Xu L et al (2020) Biodegradable materials for bone defect repair. Mil Med Res 7(54):1–25
21. Abd-Allah WM, Fathy RM (2022) Gamma irradiation effectuality on the antibacterial and bioactivity behavior of multicomponent borate glasses against methicillin-resistant *Staphylococcus aureus* (MRSA). J Biol Inorg Chem 27:155–173. https://doi.org/10.1007/s00775-021-01918-z
22. Hakki SS, Bozkurt BS, Hakki EE (2010) Boron regulates mineralized tissue-associated proteins in osteoblasts (MC3T3-E1). J Trace Elem Med Biol 24:243–250. https://doi.org/10.1016/j.jtemb.2010.03.003
23. Tunçay EÖ, Demirtaş TT, Gümüşderelioğlu M (2017) Microwave-induced production of boron-doped HAp (B-HAp) and B-HAp coated composite scaffolds. J Trace Elem Med Biol 40:72–81. https://doi.org/10.1016/j.jtemb.2016.12.005
24. Aksoy ME, Aksakal B, Aslan N, Dikici B (2021) Boron-doped hydroxyapatite coatings on NiTi alloys using the electrophoretic deposition method: enhanced corrosion and adhesion performances. J Mater Eng Perform 30:7365–7375. https://doi.org/10.1007/s11665-021-05968-x
25. Gorustovich AA, Lopez JMP, Guglielmotti MB, Cabrini RL (2006) Biological performance of boron-modified bioactive glass particles implanted in rat tibia bone marrow. Biomed Mater 100:3–9. https://doi.org/10.1088/1748-6041/1/3/002
26. Deilmann L, Winter O, Cerrutti B et al (2020) Effect of boron incorporation on the bioactivity, structure, and mechanical properties of ordered mesoporous bioactive glasses. J Mater Chem B 8:1456–1465. https://doi.org/10.1039/c9tb01805k
27. Uygulamalı S, Üniversitesi B, Fak T et al (2020) Sinterleme Yöntemiyle Apatit – Wollastonit Cam Seramik Üretimi Apatite-Wollastonite glass ceramic production by sintering method. Acad Platform J Eng Sci 8–2:217–221. https://doi.org/10.21541/apjes.656253
28. Catunda R, Vieira J, De OE (2017) Citotoxicity evaluation of three dental adhesives on vero cells in vitro. J Clin Exp Dent 9:4–9. https://doi.org/10.4317/jced.53039
29. Akshaya S, Rowlo PK, Dukle A, Nathanael AJ (2022) Antibacterial coatings for titanium implants: recent trends and future perspectives. Antibiotics 11:1–19
30. Crémet L, Broquet A, Asehnoune K, Dauvergne S et al (2015) Pathogenic potential of Escherichia coli clinical strains from orthopedic implant infections towards human osteoblastic cells. FEMS Pathog Dis 73:1–10. https://doi.org/10.1093/femspd/ftv065
31. Sharma S, Soni VP, Bellare JR (2009) Chitosan reinforced apatite–wollastonite coating by electrophoretic deposition on titanium implants. J Mater Sci Mater Med 20:1427–1436. https://doi.org/10.1007/s10856-009-3712-6
32. Nuswantoro NF, Budıman I, Septiawarman A et al (2019) Effect of applied voltage and coating time on nano hydroxyapatite coating on titanium alloy Ti6Al4V using electrophoretic deposition for orthopaedic implant application. IOP Conf Ser Mater Sci Eng 547:12004. https://doi.org/10.1088/1757-899X/547/1/012004
33. Pazarçeviren AE, Tezcaner A, Keskin D et al (2020) Boron-doped biphasic hydroxyapatite/β -tricalcium phosphate for bone tissue engineering. Biol Trace Elem Res 199:968–980

34. Uysal İ, Yılmaz B, Evis Z (2020) Boron doped hydroxyapatites in biomedical applications. Boron 5:199–208. https://doi.org/10.30728/boron.734804
35. Ramesh S, Tan C, Hamdi M et al (2007) The influence of Ca/P ratio on the properties of hydroxyapatite bioceramics. Int Soc Opt Eng. https://doi.org/10.1117/12.779890
36. Srinath P, Abdul Azeem P, Venugopal Reddy K (2020) Review on calcium silicate-based bioceramics in bone tissue engineering. Int J Appl Ceram Technol 17:2450–2464. https://doi.org/10.1111/ijac.13577
37. Chen W, Liang Y, Hou X et al (2018) Mechanical grinding preparation and characterization of TiO_2-coated wollastonite composite pigments. Materials (Basel, Switzerland). https://doi.org/10.3390/ma11040593
38. Islam MT, Felfel RM, Abou Neel EA et al (2017) Bioactive calcium phosphate-based glasses and ceramics and their biomedical applications: a review. J Tissue Eng. https://doi.org/10.1177/2041731417719170
39. Liu X, Ding C, Wang Z (2012) Apatite formed on the surface of plasma-sprayed wollastonite coating immersed in simulated body fluid. Biomaterials 22:2007–2012
40. Chen W, Liang Y, Hou X et al (2018) Mechanical grinding preparation and characterization of TiO_2-coated wollastonite composite pigments. Materials 11:1–11. https://doi.org/10.3390/ma11040593
41. Mondal S, Banthia AK (2020) Low-temperature synthetic route for boron carbide. J Eur Ceram Soc 25:287–291. https://doi.org/10.1016/j.jeurceramsoc.2004.08.011
42. Lee MH, Han MS, Kim JH (2020) A preliminary study on the roles of Fe content and neoformed Ca-rich minerals in the coloration of ceramic glazes. J Conserv Sci 36:275–283
43. Yılmaz E, Türk S (2022) Loading antibiotics on the surface of nano-networked sodium hydroxide treated titanium. Chem Pap 76:2459–2467. https://doi.org/10.1007/s11696-021-02045-4
44. Borokhov O, Schubert D (2007) Antimicrobial properties of boron derivatives. In: ACS symposium series, pp 412–435
45. Wang Y, Wang X, Li L et al (2022) An experimental and theoretical study on the photocatalytic antibacterial activity of boron-doped TiO_2 nanoparticles. Ceram Int 48:604–614. https://doi.org/10.1016/j.ceramint.2021.09.139
46. Sopchenski L, Cogo S, Eli S et al (2018) Bioactive and antibacterial boron doped TiO_2 coating obtained by PEO. Appl Surf Sci 458:49–58. https://doi.org/10.1016/j.apsusc.2018.07.049
47. Akbar W, Karagöz A, Basim GB et al (2015) Nano-boron as an antibacterial agent for functionalized textiles. Mater Res Soc Symp Proc 1793:53–57. https://doi.org/10.1557/opl.2015.728
48. Yılmaz E, Çakıroğlu B, Gökçe A et al (2019) Novel hydroxyapatite/graphene oxide/collagen bioactive composite coating on Ti16Nb alloys by electrodeposition. Mater Sci Eng C 101:292–305. https://doi.org/10.1016/j.msec.2019.03.078

Authors and Affiliations

Eren Yılmaz[1,2] · Serbülent Türk[3,4] · Alican Bahadır Semerci[5] · Mine Kırkbınar[6] · Erhan İbrahimoğlu[6] · Fatih Çalışkan[6]

✉ Eren Yılmaz
erenyilmaz@subu.edu.tr

[1] Department of Welding Technology, Arifiye Vocational High School, Sakarya Applied Sciences University, 54187 Serdivan, Sakarya, Turkey

[2] Sakarya Applied Sciences University Materials Research Center (SUMAR), 54187 Serdivan, Sakarya, Turkey

[3] Biomedical, Magnetic and Semi Conductive Materials Research Center (BIMAS-RC), Sakarya University, 54187 Serdivan, Sakarya, Turkey

[4] Biomaterials, Energy, Photocatalysis, Enzyme Technology, Nano and Advanced Materials, Additive Manufacturing, Environmental Applications and Sustainably Research and Development Group, 54187 Serdivan, Sakarya, Turkey

[5] Department of Biology, Sakarya University, 54187 Serdivan, Sakarya, Turkey

[6] Department of Metallurgical and Materials Engineering, Faculty of Technology, Sakarya University of Applied Sciences, 54187 Serdivan, Sakarya, Turkey